Domain-wall dynamics driven by adiabatic spin-transfer torques

Z. Li and S. Zhang

Department of Physics and Astronomy, University of Missouri–Columbia, Columbia, Missouri 65211, USA

In a first approximation, known as the adiabatic process, the direction of the spin polarization of currents is parallel to the local magnetization vector in a domain wall. Thus the spatial variation of the direction of the spin current inside the domain wall results in an adiabatic spin-transfer torque on the magnetization. We show that domain-wall motion driven by this spin torque has many unique features that do not exist in the conventional wall motion driven by a magnetic field. By analytically and numerically solving the Landau-Lifshitz-Gilbert equation along with the adiabatic spin torque in magnetic nanowires, we find that the domain wall has its maximum velocity at the initial application of the current but the velocity decreases to zero as the domain wall begins to deform during its motion. We have computed domain-wall displacement and domain-wall deformation of nanowires, and concluded that the spin torque based on the adiabatic propagation of the spin current in the domain wall is unable to maintain wall movement. We also introduce the concept of domain-wall inductance to characterize the capacity of the spin-torque-induced magnetic energy stored in a domain wall. In the presence of domain-wall pinning centers, we construct a phase diagram for the domain-wall depinning by the combined action of the magnetic field and the spin current.

I. INTRODUCTION

The subject of current-induced magnetization reversal (CIMR) in magnetic multilayers has received considerable interest recently.[1–8] From a fundamental point of view, this topic introduces an interaction between nonequilibrium conduction electrons and local moments, and the physics of this interaction has not been well explored. From the application point of view, the current-induced magnetization reversal opens a way to control and manipulate the magnetization dynamics that is one of the central issues in modern magnetic technologies. In conventional magnetic devices, the magnetization direction is controlled by external magnetic fields generated by a current or by a permanent magnet. These magnetic fields are usually spread over a relatively large spatial extent. The CIMR can be confined to an exact spatial region where the current flows; this property is very attractive for magnetic nanodevices, e.g., magnetic random access memory.

The physics of the current-induced magnetization reversal involves interplay between nonequilibrium conduction electrons and local magnetization; namely, the spin angular momentum carried by spin polarized electrons is transferred to the local moment through the exchange interaction. This is somewhat analogous to the well-known phenomenon of electromigration:[9] (impurity) atoms migrate in the direction opposite to the current flow. The origin of electromigration is mainly the transfer of *linear momentum* of nonequilibrium conduction electrons to atoms, resulting in a "wind force" that drives migration of the atom. For magnetic materials where the electric current is spin polarized, it is possible that the spin polarization of nonequilibrium conduction electrons changes its orientation along the direction of the current, and thus the localized magnetic moment receives a spin torque if the conduction electrons continuously transfer their spin angular momentum to the local moment in the steady state of current flow. This nonequilibrium conduction-electron-

induced spin torque can alter magnetization structures, drive magnetization dynamics, and even create domain-wall motion.

Until now, the spin-transfer model has been developed mainly on a trilayer structure where two ferromagnetic layers are separated by a spacer layer. Typically, one chooses the spacer layer thick enough to reduce the magnetic coupling between the two ferromagnetic layers and thin enough to minimize the spin-flip scattering in the spacer so that the spin-transfer torque is maximized. Several theoretical models[10–14] have been put forward to formulate the spin torque in terms of geometric and material parameters. While the correct microscopic picture of the spin torque is still under debate, all the theories contain a spin torque in the form of

$$\boldsymbol{\tau}_a = -\frac{a_J}{M_s}\mathbf{M} \times (\mathbf{M} \times \hat{\mathbf{M}}_p), \qquad (1)$$

where $\mathbf{M}$ is the magnetization of the free layer, $\hat{\mathbf{M}}_p$ is the *unit* vector along the direction of the magnetization of the pinned layer, M_s is the saturation magnetization, and a_J is a model-dependent parameter and is proportional to the current density. In general, the magnitude a_J of the spin-transfer torque is also a function of the angle between the pinned and free layer magnetization vectors.

Several theoretical attempts[15–18] have been made at understanding the unique features displayed in the spin torque Eq. (1). Here we just list three of them: (1) the spin torque may stabilize steady precessional states, i.e., the magnetization does not converge to a metastable static state even at zero temperature; (2) the spin torque may create a different stable configuration of the magnetization, e.g., an out-of-plane magnetization direction can be a solution for the metastable states; (3) the spin torque modifies the effective energy barrier or temperature in a significant and unique way.

70 024417-1

All of the above properties are derived based on the specific form of the spin torque given in Eq. (1). Equation (1) assumes that both free and pinned layers have uniform magnetization within the layers, at least along the direction of the current. In a typical ferromagnet, the magnetization is rarely uniform, and the dynamical process of magnetization is not coherent rotation in general. It would be interesting to find what the spin torque does to the magnetization dynamics of non-single-domain ferromagnets. Berger[19] introduced the "domain drag force" by considering the spin torque in a single-layer system where the magnetization is not uniform along the current. He argued, based on his intuitive physics picture, that the current can drag the domain wall along the path of the current flow. Bazaliy *et al.* proposed a spin torque in a ferromagnet within the ballistic transport model for half-metallic materials.[20] Most recently, we generalized the spin torque for any diffusive transport ferromagnet,[22]

$$\boldsymbol{\tau}_{st} = -b_J \hat{\mathbf{M}} \times [\hat{\mathbf{M}} \times (\hat{\mathbf{j}}_e \cdot \nabla)\mathbf{M}], \qquad (2)$$

where $\hat{\mathbf{M}} = \mathbf{M}/M_s$, $\hat{\mathbf{j}}_\mathbf{e} = \mathbf{j}_e/j_e$, and $b_J = Pj_e\mu_B/eM_s$, P is the spin polarization of the current, μ_B is the Bohr magneton, and j_e is the electric current density. The above torque is identical in form to that of Bazaliy *et al.*[20] However, we derived the above formulation based on a general property of ferromagnetic materials: in a ferromagnet, the spin polarization of the current is always along the direction of the local magnetization vector, i.e., the transverse component of the spin current can be neglected.[12,13,22] Thus one may define a spin current tensor $\mathcal{J} = (\mu_B/eM_s)P\mathbf{j}_e \otimes \mathbf{M}(\mathbf{r})$ where the vector $\mathbf{j}_e$ tracks the direction of the charge current and $\mathbf{M}(\mathbf{r})$ describes the direction of the spin polarization of the current. The spin-transfer torque is defined as the rate of change of the angular momentum of conduction electrons that are transferred to the local magnetization, $\boldsymbol{\tau}_{st} = d\mathbf{m}/dt = \partial\mathbf{m}/\partial t + \nabla \cdot \mathcal{J}$. In the steady state of the current flow, $\partial\mathbf{m}/\partial t = 0$ and thus we find that the above spin torque can be written as Eq. (2) if we use the fact that the magnitude of the local magnetization vector is a constant.

While the magnitude of the spin torque in spin valves, Eq. (1), depends on many unknown parameters such as interface spin-dependent resistance, the magnitude of the adiabatic spin transfer torque b_J in Eq. (2) can be accurately estimated for many ferromagnetic materials. b_J, which has the dimensions of velocity, is determined by two material parameters M_s and P; these parameters have already been determined experimentally. In Table I, we list the values of b_J for a selected set of materials for a current density $j_e = 10^7$ A/cm^2. The half metals CrO$_2$ and Fe$_2$O$_3$ have a maximum spin polarization ($P=1$) and low saturation magnetization, and thus the spin torque is larger than that of transition metals.

The paper is organized as follows. In Sec. II, we establish the equation of motion of a domain wall by using the generalized Landau-Lifshitz-Gilbert (LLG) equation along with the adiabatic torque Eq. (2). We write the equation for nanowires. In Sec. III, we propose a trial function to analytically obtain solutions for domain-wall dynamics. In particular, we address the spin-torque-induced domain propagation

TABLE I. The values of b_J for some materials for $j_e = 10^7$A/cm^2

Nanowire	M_s(A/m)	P	b_J(m/s)
Fe	17.18×10^5	0.5	1.35
Co	14.46×10^5	0.35	1.41
Ni	4.9×10^5	0.23	2.7
Permalloy	8×10^5	0.7	5.1
γ-Fe$_2$O$_3$	4.14×10^5	1.0	14.0
CrO$_2$	3.98×10^5	1.0	14.6

and distortion. Then a detailed comparison between numerical results and analytic solutions is made in Sec. IV. Finally, we summarize our major findings in Sec. V.

II. MODEL SYSTEM

We assume the current flows in the x direction along the long length of a wire, i.e., $\hat{\mathbf{j}}_\mathbf{e} = \mathbf{e}_x$. By placing this in Eq. (2) and by treating Eq. (2) as an additional torque on the standard LLG equation, we write the generalized LLG equation in the presence of the spin torque as

$$\frac{\partial \mathbf{M}}{\partial t} = -\gamma \mathbf{M} \times \mathbf{H}_{eff} + \alpha \hat{\mathbf{M}} \times \frac{\partial \mathbf{M}}{\partial t} - b_J \hat{\mathbf{M}} \times \left(\hat{\mathbf{M}} \times \frac{\partial \mathbf{M}}{\partial x} \right), \tag{3}$$

where γ is the gyromagnetic ratio, $\mathbf{H}_{eff}$ is the effective magnetic field including the external field, the anisotropy field, the magnetostatic field, and the exchange field, and α is the Gilbert damping parameter.

We now specify the geometry of the wire and the effective field entering Eq. (3). As shown in Fig. 1, the x axis is taken as the easy axis as well as the direction of the external field H_{ext}. The width and the thickness of the wire are D and d, respectively. The current is along the x direction.

We explicitly write the effective field as

$$\mathbf{H}_{eff} = \frac{H_K M_x}{M_s} \mathbf{e}_x + \frac{2A}{M_s^2} \nabla^2 \mathbf{M} - 4\pi M_z \mathbf{e}_z + H_{ext}\mathbf{e}_x, \qquad (4)$$

where H_K is the anisotropy field, A is the exchange constant, and $4\pi M_z$ is the de-magnetization field.

To gain analytical insight into the domain-wall dynamics, we first consider that the magnetization $\mathbf{M}$ varies only in the direction of the x axis. By placing Eq. (4) into Eq. (3), the LLG equation can be conveniently written in polar coordinates as
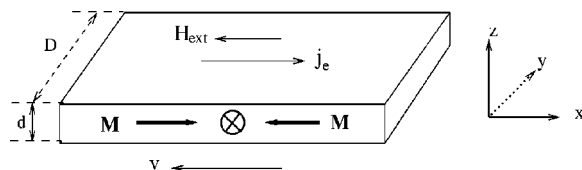
FIG. 1. Cartesian and polar coordinate systems.

$$\frac{\partial \theta}{\partial t} + \alpha \sin \theta \frac{\partial \varphi}{\partial t} = \gamma \frac{2A}{M_s} \left(2 \cos \theta \frac{\partial \varphi}{\partial x} \frac{\partial \theta}{\partial x} + \sin \theta \frac{\partial^2 \varphi}{\partial x^2} \right)$$

$$- 4\gamma \pi M_s \sin \theta \sin \varphi \cos \varphi + b_J \frac{\partial \theta}{\partial x},$$

$$(5)$$

$$\alpha \frac{\partial \theta}{\partial t} - \sin \theta \frac{\partial \varphi}{\partial t} = \gamma \frac{2A}{M_s} \left(\frac{\partial^2 \theta}{\partial x^2} - \sin \theta \cos \theta \left(\frac{\partial \varphi}{\partial x} \right)^2 \right)$$

$$- \gamma H_K \sin \theta \cos \theta$$

$$- 4\gamma \pi M_s \sin \theta \cos \theta \sin^2 \varphi - \gamma H_{ext} \sin \theta$$

$$- b_J \sin \theta \frac{\partial \varphi}{\partial x}, \qquad (6)$$

where θ represents the angle between the magnetization vector and the x axis, and φ is the out-of-plane angle of the magnetization vector projected in the yz plane, i.e., $M_z = M_s \sin \theta \sin \varphi$.

Our goal is to solve for the magnetization vector as a function of position x and time t from the above equations of motion. In the absence of a current and/or an external magnetic field, we consider that the domain wall, separated by two head-to-head domains along the wire direction, is a Néel wall[21] whose magnetization stays in the plane of the wire, i.e., $M_z = 0$, $M_x = M_s \cos \theta$, $M_y = M_s \sin \theta \cos \varphi$, where

$$\varphi = 0, \quad \theta = 2 \tan^{-1} \exp(x/W_0), \qquad (7)$$

and $W_0 = \sqrt{2A/H_K M_s}$ is the domain-wall width. At $t=0$, an electric current and/or an external field is applied. We should determine the motion of the wall at $t>0$ from Eqs. (5) and (6) by utilizing the initial condition Eq. (7).

III. ANALYTICAL RESULTS

The nonlinear partial differential equations Eqs. (5) and (6) are difficult to solve. Here we follow Walker's analysis of domain-wall motion by introducing a trial function[23]

$$\varphi = \varphi(t), \quad \ln \tan \frac{\theta}{2} = c(t) \left(x - \int_0^t v(\tau) d\tau \right). \qquad (8)$$

The first equation assumes that the projection of the magnetization vector in the domain wall on the yz plane is independent of the position. One should note that the spatial independence of $\varphi(t)$ does not mean a uniform out-of-plane component because $M_z = M_s \sin \theta \sin \varphi$ and θ varies spatially in the domain wall from $\theta = 0$ to π. The second equation in Eq. (8) postulates that the domain-wall shape remains a standard Néel-wall form except that the width of the wall $W(t) \equiv c(t)^{-1}$ varies with time and the wall moves with velocity $v(t)$. We will show later that this form of the solution is indeed a correct solution as long as the spin torque b_J and the external field H_{ext} are small.

By placing this trial function into Eqs. (5) and (6), utilizing the identities

$$\frac{\partial \varphi}{\partial x} = \frac{\partial^2 \varphi}{\partial x^2} = 0,$$

$$\frac{\partial \theta}{\partial x} = c(t) \sin \theta, \quad \frac{\partial^2 \theta}{\partial x^2} = c(t)^2 \sin \theta \cos \theta,$$

$$\frac{\partial \theta}{\partial t} = c_1(x,t) \sin \theta,$$

and defining a function $c_1(x,t)$,

$$c_1(x,t) \equiv \frac{dc(t)}{dt} \left(x - \int_0^t v(\tau) d\tau \right) - c(t) v(t), \qquad (9)$$

we find

$$c_1(x,t) + \alpha \frac{d\varphi}{dt} = -4\pi \gamma M_s \sin \varphi \cos \varphi + b_J c(t) \qquad (10)$$

$$- \alpha c_1(x,t) + \frac{d\varphi}{dt} - \gamma H_{ext}$$

$$= \gamma \left(H_K - \frac{2A}{M_s} c(t)^2 + 4\pi M_s \sin^2 \varphi \right) \cos \theta. \qquad (11)$$

Strictly speaking, Eqs. (10) and (11) cannot be valid because $c_1(x,t)$ defined in Eq. (9) is linearly proportional to x but there are no other terms in Eq. (10) and (11) containing the spatial variable x. Thus, a trial function of the form of Eq. (8) is possible only when one discards the spatial dependence of c_1. Equivalently, the first term on the right side of Eq. (9) must be much smaller compared to the second term so that $c_1 \approx -c(t)v(t)$. While one could not determine the smallness of this first term *a priori*, we will later confirm that $W(t)$ shrinks by only a few percent during the domain-wall motion and varies slowly with time so that $dc(t)/dt$ is indeed small. Now the left-hand side of Eq. (11) becomes x independent and thus the prefactor in front of $\cos \theta$ on the right-hand side of Eq. (11) must be identically zero,

$$H_K - \frac{2A}{M_s} c(t)^2 + 4\pi M_s \sin^2 \varphi = 0 \qquad (12)$$

and

$$\alpha c(t) v(t) + \frac{d\varphi}{dt} = \gamma H_{ext}. \qquad (13)$$

By placing Eq. (13) into Eq. (10), we have

$$(1 + \alpha^2) \frac{d\varphi}{dt} = \gamma H_{ext} + \alpha b_J c(t) - 4\pi \alpha \gamma M_s \sin \varphi \cos \varphi. \qquad (14)$$

Equations (12) and (14) are the ordinary first-order differential equations that determine the domain-wall width $c^{-1}(t)$ and the rotation of the domain-wall plane $\varphi(t)$ subject to the initial values $\varphi(t=0)=0$ and $c^{-1}(t=0)=W_0$. Once these two equations are solved, we can obtain the velocity of the domain wall from Eq. (13):
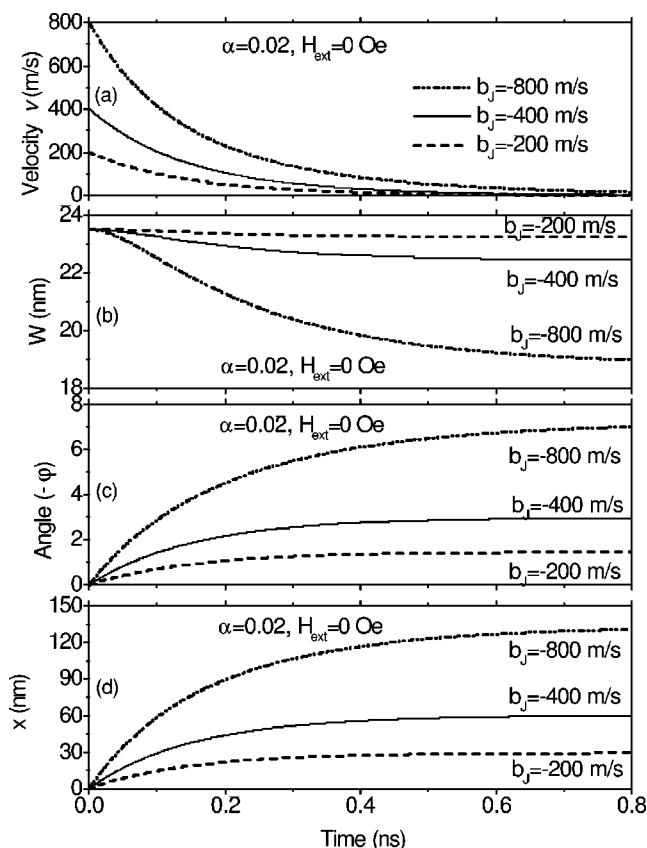
FIG. 2. The velocity v, the wall width W, the wall angle φ, and the displacement x as a function of time t for different spin torques and for $H_{ext}=0$ Oe. The parameters are $4\pi M_s=1.8\times10^4$ Oe, $H_K=500$ Oe, $M_s=14.46\times10^5$ A/m, $A=2.0\times10^{-11}$ J/m, and $\alpha=0.02$.

$$v(t) = \frac{\gamma(\alpha H_{ext} + 4\pi M_s \sin\varphi \cos\varphi)}{(1+\alpha^2)c(t)} - \frac{b_J}{1+\alpha^2}. \quad (15)$$

The numerical solutions of Eqs. (12) and (14) are represented in Fig. 2, where the domain-wall velocity, displacement, and distortion are shown as a functions of time. In the following subsections, we discuss these quantities.

A. Domain-wall velocity

At $t=0$, the wall is a standard in-plane Néel wall, i.e., $\varphi(t=0)=0$. From Eq. (15), we have readily seen that the velocity is $-b_J/(1+\alpha^2)$ at the initial application of the current if no external field is applied. On the other hand, for $t\rightarrow\infty$, $d\varphi/dt=0$. We immediately find, from Eq. (13),

$$v_s \equiv v(\infty) = \frac{\gamma H_{ext}}{c(\infty)\alpha}; \quad (16)$$

this result is the same as that of Schryer and Walker[23] in the absence of the spin torque. We conclude that the terminal velocity is completely independent of the spin torque. This implies that the spin current alone, i.e., no applied field, cannot move the domain wall to a large distance. In Fig. 2(a), the velocity of the domain wall during the application of the current is shown. It is noted that the domain-wall motion stops at a fraction of a nanosecond.

B. Domain-wall distortion

In our analytical theory, domain-wall distortion is characterized by two parameters $\varphi(t)$ and $c^{-1}(t)$. The former describes the out-of-plane component of the magnetization and the latter is the time-dependent domain-wall width. When $t\rightarrow\infty$, the distortion is maximum. By setting $d\varphi/dt=0$, we find $\varphi(\infty)$ from Eq. (14) in the absence of the external field,

$$\sin 2\varphi(\infty) = \frac{b_J c(\infty)}{2\gamma\pi M_s} = \frac{b_J\sqrt{H_K M_s/2A + (4\pi M_s^2/2A)\sin^2\varphi(\infty)}}{2\gamma\pi M_s} \quad (17)$$

where the last identity is from Eq. (12). When b_J ($\ll\gamma W_0\sqrt{4\pi M_s H_K}$) is small, $\sin\varphi\approx\varphi$ and $\sin^2\varphi\approx0$, and Eq. (17) is simplified as

$$\varphi(\infty) \approx \frac{b_J}{4\pi\gamma M_s W_0}. \quad (18)$$

By inserting this into Eq. (12) and again by assuming b_J is small, we find the maximum reduction of the domain-wall width as

$$\frac{W(\infty)}{W_0} = 1 - \frac{1}{2W_0^2}\frac{b_J^2}{4\pi M_s H_K \gamma^2}. \quad (19)$$

In Figs. 2(b) and 2(c), we show the domain-wall distortion during the application of the current.

C. Domain-wall displacement

As the domain-wall motion eventually stops even for a perfect wire in the absence of an external field, it is interesting to see how far the domain wall moves, i.e., what is the maximum distance a domain wall can travel before it stops? We estimate this displacement by integrating the velocity and utilizing Eqs. (12) and (13):

$$x_{max} = \int_0^\infty v\, dt = -\int_0^{\varphi(\infty)}\frac{d\varphi}{\alpha c} \approx -\frac{b_J}{4\pi\gamma\alpha M_s}. \quad (20)$$

Notice that the displacement is inversely proportional to the damping constant. In Fig. 2(d), we show the displacement as a function of time.

D. Inductance of domain wall

We have seen that domain-wall motion driven by a current is very different from that driven by an external field. In the latter case, the initial velocity upon the application of the external field is small and the velocity gradually increases until a saturation velocity is reached; after that, the domain wall moves with a constant velocity. We can understand this field-driven wall motion rather straightforwardly: the wall motion along the direction of the field is to reduce the Zeeman energy; the rate of Zeeman energy reduction equals the energy damping in a constantly moving domain wall. For the current-driven domain-wall motion, the wall motion does not decrease the energy because the spin torque has no effect on the *uniformly* magnetized domains. Instead, the application

of the spin torque introduces energy to the wall so that distortion of the wall occurs. The consequence of the wall distortion is to generate an energy damping mechanism so that pumping of the energy by the spin torque can be compensated by the damping. Once the dynamic equilibrium between pumping and damping is reached, the domain-wall motion stops and the distortion is maximum. To quantitatively see this interesting feature, we consider the wall energy

$$E = \int_{-\infty}^{\infty} \left\{ 2\pi M_z^2 - \frac{H_K}{2M_s} M_x^2 + \frac{A}{M_s^2} \left| \frac{\partial \mathbf{M}}{\partial x} \right|^2 \right\} dx, \quad (21)$$

where the first term is the magnetostatic energy, the second is the anisotropy energy, and the final term is the exchange energy. The rate of energy change can be obtained via $dE = -\mathbf{H}_{eff} \cdot d\mathbf{M}$ and use of the LLG equation,

$$\frac{dE}{dt} = \int_{-\infty}^{\infty} \left\{ -\frac{\gamma\alpha}{1+\alpha^2} \frac{1}{M_s} |\mathbf{M} \times \mathbf{H}_{eff}|^2 - \frac{b_J}{1+\alpha^2} \mathbf{H}_{eff} \cdot \frac{\partial \mathbf{M}}{\partial x} \right.$$
$$\left. - \frac{b_J}{1+\alpha^2} \frac{\alpha}{M_s} \frac{\partial \mathbf{M}}{\partial x} \cdot (\mathbf{H}_{eff} \times \mathbf{M}) \right\} dx. \quad (22)$$

Note that the first term is pure damping; the second and third terms are the result of the spin torque. By inserting the effective field Eq. (4), we can express the above two equations in terms of the wall distortion parameters $\varphi(t)$ and $c(t)$. The expression is algebraically tedious and lengthy; we do not write it down here. Instead, we simply consider limiting cases where the spin torque is small. A straightforward calculation leads to simple but insightful expressions for the rate of the energy change and the wall energy,

$$\frac{dE}{dt} = \frac{16\mu_0 \pi W_0 M_s^2}{3} \sin\varphi \cos\varphi \frac{d\varphi}{dt} \quad (23)$$

and

$$\Delta E \equiv E(b_J) - E(0) = \frac{1}{2} L_w b_J^2, \quad (24)$$

where we have defined the inductance of the domain wall $L_w = \pi/(3\mu_0 \gamma^2 W_0)$. These expressions illustrate the energy process during the domain-wall motion. The total spin-current-induced wall energy is proportional to the square of the current density—in analogy with the inductance of a circuit.

The domain-wall energy stored in the form of domain-wall distortion can be released once the spin current is turned off—in analogy with the electric discharge of inductance. In fact, we can easily show that the domain wall will move back to its original location. To see this, we set $b_J = 0$ in Eq. (15) and the velocity for $H_{ext} = 0$ is

$$v_{rec}(t) = \frac{\gamma 4\pi M_s \sin\varphi \cos\varphi}{(1+\alpha^2)c(t)}. \quad (25)$$

Note that the initial condition is now $\varphi = \varphi(\infty)$ and the initial velocity is $+b_J/(1+\alpha^2)$. By dropping the first two terms in the right-hand side of Eq. (14), one can integrate $\varphi(t)$ out from Eq. (14) and it is easy to check that

$$x_{rec} \equiv \int_0^{\infty} v_{rec} dt = \int_{\varphi(\infty)}^0 \frac{d\varphi}{\alpha c} = -x_{max}. \quad (26)$$

The domain wall moves to its original position. Again, this phenomenon is analogous to the discharge of an inductance in the usual electronic circuit. We will show in the next section how this feature differs from the domain-wall motion when an external field is turned off.

E. Beyond Walker's limit

Until now, our analysis is based on Walker's trial function. As in the case of field-driven domain-wall motion, it is essential to assume that the deviation from the original Néel wall is small. This limits the validity of our analytical result to a small current density. In this subsection, we show that when the current density is larger than a critical current, Walker's trial function fails to describe the domain-wall motion. In fact, the domain wall will not stop at a sufficient large current and the distortion of the domain wall can no longer be simply described by two parameters [$\varphi(t)$ and $c(t)$]. Fortunately, for the experimentally interesting regime, the applied current density is usually within the applicability of Walker's theory.

To find the critical current density b_c, we consider a time-independent solution by setting $d\varphi/dt = 0$ in Eq. (14). By using Eq. (12), we find

$$b_J = \frac{4\pi\gamma M_s \sin\varphi \cos\varphi}{\sqrt{H_K M_s/2A + (4\pi M_s^2/2A)\sin^2\varphi}}. \quad (27)$$

Maximizing b_J with respect to the angle φ, we have

$$\sin^2\varphi_c = \frac{H_K}{2H_K + 4\pi M_s}, \quad (28)$$

$$\sin\varphi_c \cos\varphi_c = \frac{\sqrt{H_K(H_K + 4\pi M_s)}}{2H_K + 4\pi M_s}. \quad (29)$$

Inserting Eqs. (28) and (29) into Eq. (27), we find that the maximum spin torque for a stationary solution is

$$b_c = \frac{4\pi\gamma M_s \sqrt{H_K + 4\pi M_s}}{\sqrt{(M_s/2A)(2H_K + 4\pi M_s)^2 + (4\pi M_s^2/2A)(2H_K + 4\pi M_s)}} \quad (30)$$

when $4\pi M_s \gg H_K$, and

$$b_c \approx 4\pi\gamma M_s \xi \quad (31)$$

where $\xi = \sqrt{A/(4\pi M_s^2)}$ is the exchange length. Thus when $b_J > b_c$ the stationary solution of Schryer and Walker fails. On the other hand, if the spin torque is smaller than b_c, the maximum distortion shown in Eq. (28) is small and thus the Schryer and Walker trial function is valid. For a Co nanowire, $4\pi M_s = 1.8 \times 10^4$ Oe, $H_K = 500$ Oe, $\gamma = 1.9 \times 10^7$ Oe^{-1} s^{-1}, $M_s = 14.46 \times 10^5$ A/m, and $A = 2.0 \times 10^{-11}$ J/m, and the critical current is about $b_c = 922$ m/s or $j_e^c = 2.2 \times 10^{10}$ A/cm^2. This current density is at least one to two orders of magnitude larger than typical experimental val-
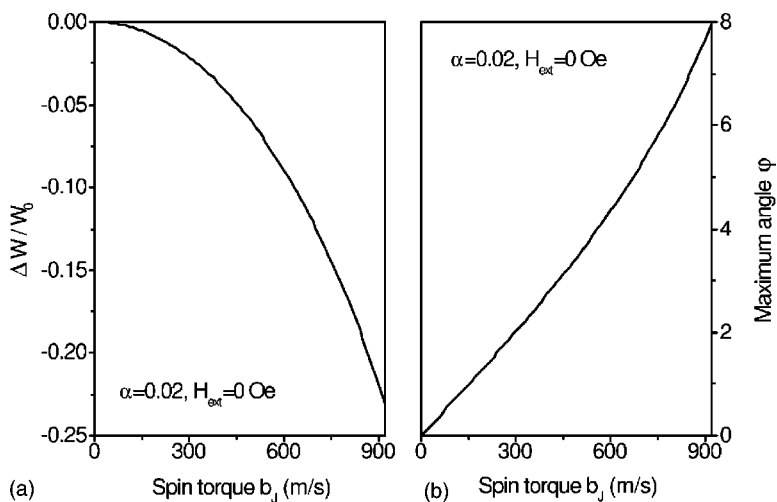
FIG. 3. Maximum wall width narrowing $\Delta W/W_0$ and the maximum angle φ as a function of the spin torque.

ues and thus the trial function and its solutions are applicable to most of the experiments. In Fig. 3, we show the maximum deformation of the domain wall; even for a current density as high as 2×10^{10} A/cm^2, the maximum angle φ is about 8° and the wall shrinks by only 22%. Thus we confirm that the trial functions are good approximations for the domain-wall dynamics at least in the one-dimensional model presented in this section.

IV. NUMERICAL RESULTS

Until now, our description of domain-wall dynamics is based on the assumption that the out-of-plane angle φ is time dependent but spatially independent. For a realistic nanowire, there are a number of complications. Among them, the magnetization varies along the direction of the wire width, i.e., one needs to go beyond Schryer and Walker's one-dimensional (1(D)) model. Furthermore, a realistic wire is expected to contain various pinning centers, and it would be interesting to see the effect of pinning on domain-wall motion. In general, a micromagnetic calculation is required to include these complications and to address the role of magnetostatic energy (except the shape anisotropy perpendicular to the film) discarded in our analytical model. In the follow-ing numerical calculation, we consider the example of a Co nanowire whose dimensions are as follows: the thickness is $d=5$ nm, the width is $D=200$ nm, and the length is 1.2 μm. The small thickness and large width would make a 1d calculation approximately valid. To made our numerical calculation directly comparable with the analytical results obtained in the last section, we include the demagnetizing field only through the shape anisotropy. We numerically integrate out Eqs. (5) and (6) by using a fourth-order predictor-corrector method with an 0.8 ps time step. Initially, at $t=0$, a stationary Néel wall is centered at $x=0$, a spin current is turned on along the x direction, and the external field is also applied along the x direction at $t>0$.

In the presence of the spin torque, the magnetization of the domain wall is no longer confined in the plane of the layer and the original Néel wall is distorted during the motion of the domain wall. In Fig. 4, we show snapshots of magnetization patterns at $t=0.06$ ns after the current is turned on at $t=0$. For a small current density, the shape of the Néel wall is essentially unchanged except for a small out-of-plane magnetization, consistent with our analytical model in the previous section. When the applied current is increased to values larger than the critical current, the shape of the Néel wall is completely destroyed. The magnetization inside the wall has developed a significant out-of-plane component [see
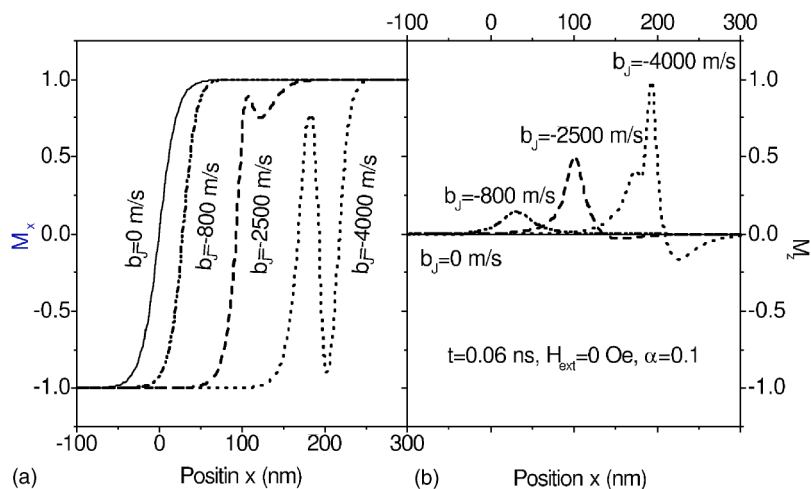
FIG. 4. Snapshots of the moving magnetic wall at $t=0.06$ ns in a Co nanowire. The damping constant $\alpha=0.1$ and the external field $H_{ext}=0$ Oe.
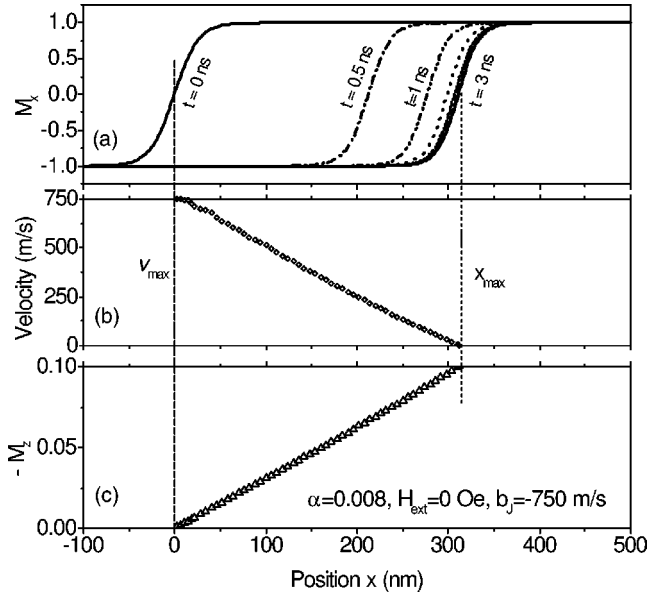
FIG. 5. (a) The wall positions at several times $t=0$, 0.5 ns, 1.0 ns, 1.5 ns, 2.0 ns, 2.5 ns, and n=3.0 ns; (b) the wall velocity as a function of the wall position; (c) the maximum out-of-plane component of the magnetization as a function of the wall position. The damping constant is $\alpha=0.008$, the spin torque is $b_J=-750$ m/s, and the external field $H_{ext}=0$ Oe.

Fig. 4(b)], and the wall has split into complicated multiple walls. In our calculation, the critical spin torque $b_c \approx 1240$ m/s, which approximately agrees with our analytical result from Eq. (30). We now confine our discussion below to the case where the current density is smaller than the critical current.

For a perfect wire, the Néel wall moves with a velocity $v=-b_J$ immediately after the application of the current. In
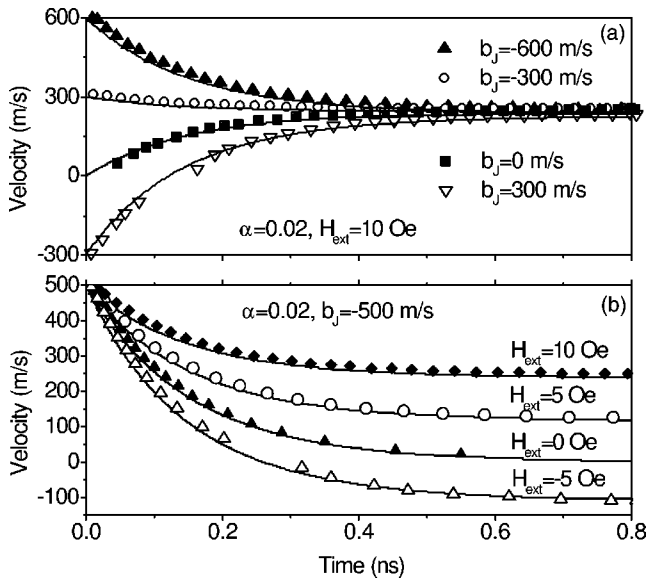
FIG. 6. Domain-wall velocity as a function of time (a) for different spin torques at a fixed magnetic field (10 Oe), and (b) for different magnetic fields at a fixed spin torque ($b_J=-500$ m/s). The solid curves represent the analytical results and the scattered points are the numerical solutions.
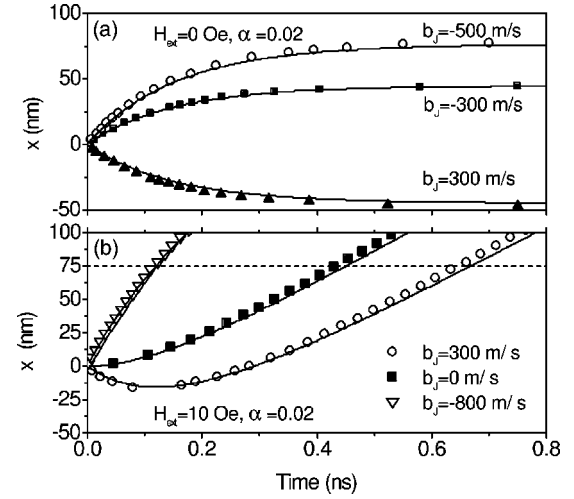
FIG. 7. Displacement of the domain wall for several spin torques without (a) and with (b) the external field. The solid curves represent the solutions of the trial function and the scattered points are the numerical results.

Fig. 5, we show the wall positions at different times as the well as the wall velocity and wall distortion when the wall moves to different positions. The domain wall remains a quasi-Néel wall and eventually the wall completely stops. At $x=0$, the wall velocity is at its maximum ($v_{max}=750$ m/s). When the wall stops, the maximum out-of-plane component of the magnetization (M_z component) approaches ($|M_z|/M_s =0.1$) and the total displacement is $x_{max}=312$ nm.

It is interesting to take a look at the domain-wall dynamics with simultaneous application of the current and the external field. As we already pointed out the initial domain-wall velocity is determined by the current but the final terminating velocity is controlled by the external field (see Fig. 6). We confirm here that the spin torque alone is unable to move the domain wall over a long distance (see Fig. 7(a)). This feature is just opposite to the domain-wall motion
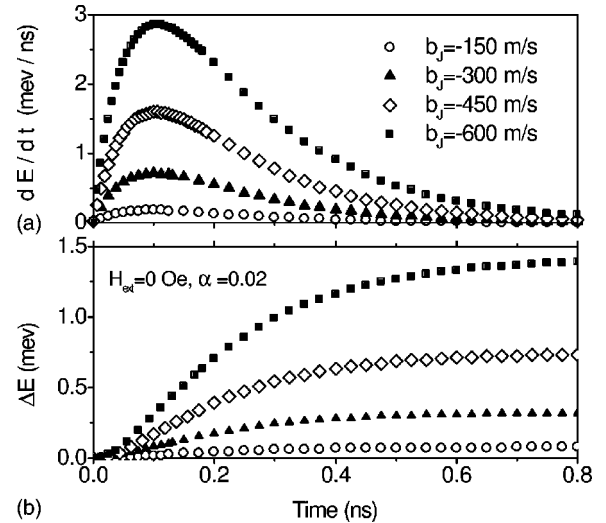
FIG. 8. Energy power (a) and net energy gain (b) of the domain wall as a function of time.
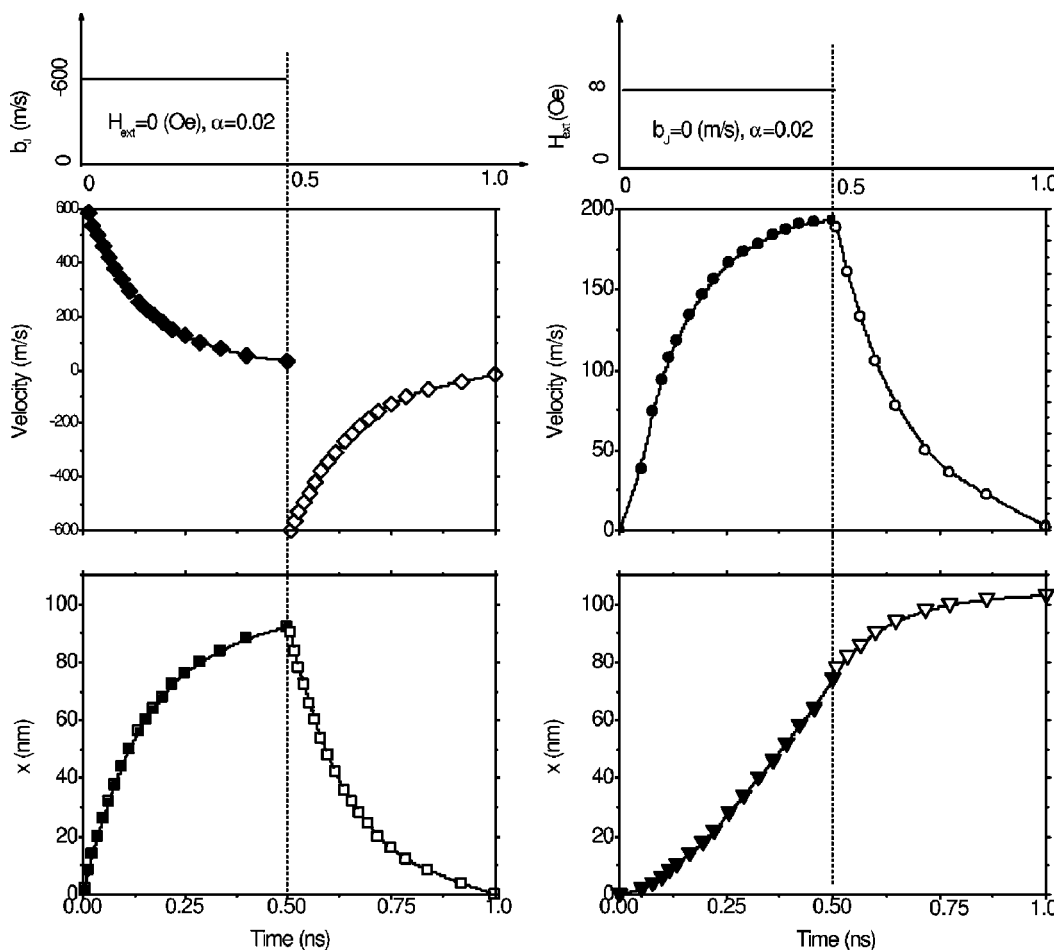
FIG. 9. Velocity v and displacement x for a pulsed spin current (left panels) and for a pulsed magnetic field (right panels). The damping constant is $\alpha=0.02$.

driven by an external field: at an initial application of the magnetic field, the wall velocity is small [in fact one can easily show that it is $\alpha H_{ext} W_0/(1+\alpha^2)$ from Eq. (15)], but it becomes faster and faster until it reaches the saturated speed

FIG. 10. The phase boundary of pinning and depinning domain walls for two types of pinning centers; see text for the definition of the pinning parameters V_0 and ζ. The external field is applied along the $-x$ direction and the spin current is along the $+x$ direction at $t=0$. The damping constant is $\alpha=0.02$.

from Eq. (16) at $\nu_s=\gamma H_{ext} W(\infty)/\alpha$. The origin of this difference was discussed at great length in the last section. The fact that the initial domain-wall velocity is determined by the current but the final terminating velocity is controlled by the external field can be used to design high- and low-speed domain-wall propagation by properly choosing the desired spin current density and the magnetic field. For example, if we are to move the domain wall by 75 nm, the magnetic field (10 Oe) alone will take 0.43 ns. With the help of the spin torque $b_J=-800$ m/s, the same displacement can be made in 0.11 ns and it takes 0.65 ns when $b_J=300$ m/s. These features are clearly illustrated in Fig. 7(b).

We show the rate of energy input of the domain wall during the application of the spin torque in Fig. 8. The rate of energy pumping from the spin torque increases at the initial application of the spin current; then it develops a maximum rate. After that, the rate decreases due to increase of the damping. Finally, the energy pumping is exactly compensated by the damping and the wall motion stops.

It is interesting to compare our calculations with experiment[24] where a domain-wall speed of about 3 m/s for a current density 1.2×10^8 A/cm^2 was observed. As we have concluded that the spin torque alone is unable to move the wall over a long distance (1 μm), the observed domain-wall velocity over large distances must come from three possible

scenarios. (1) An additional magnetic field generated by the current (Oersted field) was present in the experiment. One just needs a very small magnetic field to generate this low-velocity domain-wall motion. In fact, 1–2 Oe was sufficient and it was hard to rule out such a small field in the experiment. (2) There is a possibility of another spin-current-induced torque which has a different form from Eq. (2). Indeed, if one relaxes the adiabatic process which assumes that the direction of the spin polarization of the current adiabatically follows the magnetization vector in the domain wall, one generates an other spin torque. A detailed calculation of the spin torque from nonadiabatic processes is beyond the scope of the present work; we will defer it to a future publication. (3) We need to emphasize that the domain-wall motion in the present theory relies on the form of the Gilbert damping term. If we replace the Gilbert damping in Eq. (3) by a Landau-Lifshitz damping, i.e., $\alpha\gamma\mathbf{M}\times(\mathbf{M}\times\mathbf{H}_{eff})$, we obtain a finite velocity independent of the damping parameter. Again, we should defer this subtle difference to a further study. We point out that the other existing experiments[25,26] seem to support our model: they report that a magnetic field is always required to move the wall over a long distance.

We end the section by looking at two more interesting examples. The first one is that the spin current is applied in the form of a pulse. If we apply a rectangular pulsed spin current along the x direction, what dynamic behaviors do the domain walls have? In Fig. 9, we show the evolution of velocity $v(t)$ and displacement $x(t)$ with the pulsed spin torque and we compared them with the pulsed magnetic field. Suppose a spin torque with magnitude $b_J = -600$ m/s is turned on at $t=0$ and turned off at $\tau=0.5$ ns. In the absence of the external field, the domain wall moves back to its original location after the current is turned off. This is again consistent with our analytical result. However, for the field-driven domain-wall motion, the domain wall continues to move in the forward direction after the field is turned off.

Another example is to model the effect of pinning centers in the domain-wall motion. In realistic nanowires, domain walls are not completely free to move. There are various pinning sources such as defects and roughness. We introduced a pinning field $H_{pin} = V_0 x H(\zeta - |x|)/\zeta$, where $H(y)$ is the Heaviside step function, $\zeta > 0$ is the distance from the domain wall center, and x is the position. In Fig. 10, we present the result for the critical magnetic field required to move the wall in the presence of a defect. The role of the current is to first move the domain wall out of the pinning center so that the critical magnetic field required to move the wall is smaller.

V. CONCLUSIONS

We have demonstrated in this paper that the domain-wall motion driven by a spin current has many unique features that do not exist in the conventional domain-wall motion driven by a magnetic field. We solved the Landau-Lifshitz-Gilbert equation along with the current-induced spin torque; we summarize below our main findings; which are supported by our analytical and numerical study. (1) The spin torque alone can move the domain wall, but the total displacement is limited, thus the spin torque is not capable of moving domain walls over a large distance. (2) Since the speed of the wall is large at the initial application of the spin torque, there the spin torque has an advantage over the magnetic field for wall movement at short distances.(3) The domain wall is capable of storing current-induced energy and thus the energy process of the domain wall is very similar to the charge and discharge of inductance in an electric circuit. (4) The spin torque can help to reduce the critical field needed to move a domain wall if domain-wall pinning centers are present. (5) It may be important to extend the work to a spin torque other than the adiabatic spin torque used here in order to study the contribution from a nonadiabatic spin torque whose form has not yet been investigated.

In conclusion, a spin torque with the form of Eq. (2) is proposed to study the dynamics of domain walls. Due to the different roles played by the spin torque and by the external field, the current-driven domain-wall motion represents a different type of torque. This spin torque creates the opportunity for fast domain-wall motion using the combined field and spin torque.

Note added in proof. Recently, a paper was published,[27] in which the critical current of domain wall motion was briefly discussed.

[1] J. A. Katine, F. J. Albert, R. A. Buhrman, E. B. Myers, and D. C. Ralph, Phys. Rev. Lett. **84**, 3149 (2000).

[2] J. Grollier, V. Cros, A. Hamzic, J. M. George, H. Jaffres, A. Fert, G. Faini, J. Ben Youssef, and H. Legall, Appl. Phys. Lett. **78**, 3663 (2001).

[3] B. Özyilmaz, A. D. Kent, D. Monsma, J. Z. Sun, M. J. Rooks, and R. H. Koch, Phys. Rev. Lett. **91**, 067203 (2003).

[4] S. Urazhdin, N. O. Birge, W. P. Pratt, Jr., and J. Bass, Phys. Rev. Lett. **91**, 146803 (2003).

[5] M. Tsoi, V. Tsoi, J. Bass, A. G. M. Jansen, and P. Wyder, Phys. Rev. Lett. **89**, 246803 (2002).

[6] S. I. Kiselev, J. C. Sankey, I. N. Krivorotov, N. C. Emley, R. J. Schoelkopf, R. A. Buhrman, and D. C. Ralph, Nature (London) **425**, 380 (2003).

[7] R. H. Koch, J. A. Katine, and J. Z. Sun, Phys. Rev. Lett. **92**, 088302 (2004).

[8] M. R. Pufall, W. H. Rippard, and T. J. Silva, Appl. Phys. Lett. **83**, 323 (2003).

[9] For a review, see, e.g., R. S. Sorbello, in *Solid State Physics*, edited by H. Ehrenreich and F. Spaepen (Academic Press, New York, 1998), Vol. 51, p. 159, and references therein.

[10] J. Slonczewski, J. Magn. Magn. Mater. **159**, L1 (1996); **195**,

L261 (1999).

[11] X. Waintal, E. B. Myers, P. W. Brouwer, and D. C. Ralph, Phys. Rev. B **62**, 12 317 (2000).

[12] M. D. Stiles and A. Zangwill, Phys. Rev. B **66**, 014407 (2002).

[13] A. Brataas, Y. V. Nazarov, and G. E. W. Bauer, Phys. Rev. Lett. **84**, 2481 (2000).

[14] S. Zhang, P. M. Levy, and A. Fert, Phys. Rev. Lett. **88**, 236601 (2002).

[15] J. Sun, Phys. Rev. B **62**, 570 (2000).

[16] Ya. B. Bazaliy, B. A. Jones, and S.-C. Zhang, J. Appl. Phys. **89**, 6793 (2001).

[17] J. Miltat, G. Albuquerque, A. Thiaville, and C. Vouille, J. Appl. Phys. **89**, 6982 (2001).

[18] Z. Li and S. Zhang, Phys. Rev. B **68**, 024404 (2003); Phys. Rev. B **69**, 134416 (2004).

[19] L. Berger, J. Appl. Phys. **49**, 2156 (1978); **55**, 1954 (1984);

[20] Ya. B. Bazaliy, B. A. Jones, and S.-C. Zhang, Phys. Rev. B **57**, R3213 (1998).

[21] A. Hubert and R. Schafer, *Magnetic Domains* (Springer, Berlin, 1998).

[22] Z. Li and S. Zhang, Phys. Rev. Lett. **92**, 207203 (2004).

[23] N. L. Schryer and L. R. Walker, J. Appl. Phys. **45**, 5406 (1974).

[24] A. Yamaguchi, T. Ono, S. Nasu, K. Miyake, K. Mibu, and T. Shinjo, Phys. Rev. Lett. **92**, 077205 (2004).

[25] J. Grollier, P. Boulenc, V. Cros, A. Hamzić, A. Vaurés, A. Fert, and G. Faini, Appl. Phys. Lett. **83**, 509 (2003).

[26] M. Tsoi, R. E. Fontana, and S. S. P. Parkin, Appl. Phys. Lett. **83**, 2261 (2003).

[27] G. Tatara and H. Kohno, Phys. Rev. Lett. **92**, 086601 (2004).